Activation of a camptothecin prodrug by specific carboxylesterases as predicted by quantitative structure-activity relationship and molecular docking studies

Kyoung Jin P. Yoon,[1] Erik J. Krull,[1] Christopher L. Morton,[1] William G. Bornmann,[3] Richard E. Lee,[2] Philip M. Potter,[1] and Mary K. Danks[1]

[1]Department of Molecular Pharmacology, St. Jude Children's Research Hospital; [2]Department of Pharmaceutical Sciences, University of Tennessee Health Science Center, Memphis, TN; and [3]Memorial Sloan-Kettering Cancer Center, New York, NY

Abstract

7-Ethyl-10-[4-(1-piperidino)-1-piperidino]carbonyloxycamptothecin (irinotecan, CPT-11) is a camptothecin prodrug that is metabolized by carboxylesterases (CE) to the active metabolite 7-ethyl-10-hydroxycamptothecin (SN-38), a topoisomerase I inhibitor. CPT-11 has shown encouraging antitumor activity against a broad spectrum of tumor types in early clinical trials, but hematopoietic and gastrointestinal toxicity limit its administration. To increase the therapeutic index of CPT-11 and to develop other prodrug analogues for enzyme/prodrug gene therapy applications, our laboratories propose to develop camptothecin prodrugs that will be activated by specific CEs. Specific analogues might then be predicted to be activated, for example, predominantly by human liver CE(hCE1), by human intestinal CE (hiCE), or in gene therapy approaches using a rabbit liver CE (rCE). This study describes a molecular modeling approach to relate the structure of rCE-activated camptothecin prodrugs with their biological activation. Comparative molecular field analysis, comparative molecular similarity index analysis, and docking studies were used to predict the biological activity of a 4-benzylpiperazine derivative of CPT-11 [7-ethyl-10-[4-(1-benzyl)-1-piperazino]carbonyloxycamptothecin (BP-CPT)] in U373MG glioma cell lines transfected with plasmids encoding rCE or hiCE. BP-CPT has been reported to be activated more efficiently than CPT-11 by a rat serum esterase activity; however, three-dimensional quantitative structure-activity relationship studies predicted that rCE would activate BP-CPT less efficiently than CPT-11. This was confirmed by both growth inhibition experiments and kinetic studies. The method is being used to design camptothecin prodrugs predicted to be activated by specific CEs. (Mol Cancer Ther. 2003;2:1171–1181)

Received 5/14/03; revised 6/19/03; accepted 8/15/03.

The costs of publication of this article were defrayed in part by the payment of page charges. This article must therefore be hereby marked advertisement in accordance with 18 U.S.C. Section 1734 solely to indicate this fact.

Grant support: In part by NIH grants CA76202, CA79765, CA23099, and CA21765, by the American Lebanese and Syrian Associated Charity, and by the College of Pharmacy, University of Tennessee Health Science Center (R.E.L.).

Requests for Reprints: Mary K. Danks, Department of Molecular Pharmacology, St. Jude Children's Research Hospital, 332 North Lauderdale, Memphis, TN 38015. Phone: (901) 495-3440; Fax: (901) 495-4293. E-mail: mary.danks@stjude.org

Introduction

In theory, therapeutic approaches designed to achieve tumor cell-selective activation of nontoxic prodrugs have the potential to produce tumor-specific cell kill. To be successful in practice, however, the enzymes and prodrugs comprising these approaches should fulfill several essential criteria. These include a significant difference in potency between the prodrug and the active metabolite and a relative inefficiency of prodrug activation by ubiquitously expressed endogenous human enzymes compared with the enzyme exploited in the enzyme/prodrug therapeutic approach. Two exogenous enzyme/prodrug combinations have been investigated extensively: *Herpes simplex* virus thymidine kinase/ganciclovir (1–4) and *Escherichia coli* cytosine deaminase/5-fluorocytosine (5–7). Recently, our laboratories have described the potential use of rabbit liver carboxylesterase (rCE) with the camptothecin analogue 7-ethyl-10-[4-(1-piperidino)-1-piperidino]carbonyloxycamptothecin (irinotecan, CPT-11; 8, 9).

rCE activates CPT-11 more efficiently than any enzyme thus far identified (9, 11, 12), and its expression sensitizes primary neuroblastoma cells to this prodrug (10). 7-Ethyl-10-hydroxycamptothecin (SN-38), the active form of CPT-11, is up to 1000-fold more potent than CPT-11 (13). A previous report by Tsuji *et al.* described several additional camptothecin prodrugs (14). One analogue in particular, a 4-benzylpiperazine derivative, was activated 7-fold more efficiently than CPT-11 by a rat serum esterase activity, suggesting that it might be possible to identify camptothecin analogues that would be preferentially activated by specific esterases. Relevant to this study, rCE is 76% similar to rat serum esterase at the amino acid level. CPT-11 is also activated by two known human enzymes, human intestinal CE (hiCE) and human liver CE-1 (hCE1), but activation of this prodrug *in vivo* is relatively inefficient (15–17).

Therefore, based in part on the data of Tsuji *et al.*, we synthesized the 4-benzylpiperazine derivative of SN-38, 7-ethyl-10-[4-(1-benzyl)-1-piperazino]carbonyloxycamptothecin(BP-CPT), performed three-dimensional quantitative structure-activity relationship (QSAR) and docking studies, and compared the ability of CPT-11 and BP-CPT to inhibit growth of U373MG human glioma cells

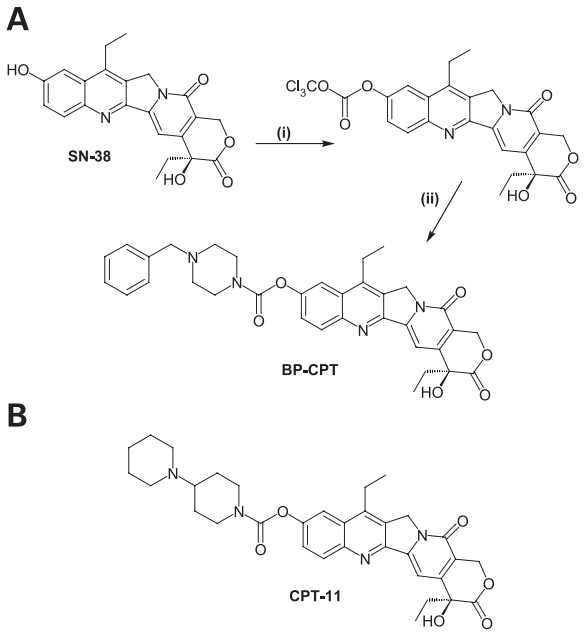

Figure 1. A, synthetic scheme of BP-CPT. Reagents and reaction conditions for each synthetic step are detailed in ''Materials and Methods.'' **B,** chemical structure of CPT-11.

transfected to express rCE or hiCE. K_m values and catalytic efficiencies were also determined. The results of this study are being used as the basis for designing other camptothecin prodrugs for virus- and antibody-directed enzyme prodrug therapy (VDEPT and ADEPT) approaches.

Materials and Methods

Chemicals

CPT-11 was provided by Dr. J. P. McGovren (Pharmacia & Upjohn, Kalamazoo, MI). A 10-mM stock solution in 100% methanol was stored at −20°C and was diluted immediately before use. All other chemicals and supplies were obtained from Sigma-Aldrich Chemical Co. (Milwaukee, WI), unless otherwise indicated.

Chemical Synthesis

SN-38 was prepared from the modified method by Wood *et al.* (18). BP-CPT was synthesized using SN-38 as a starting material by method previously used for syntheses of nitrophenol derivatives (19). The synthetic scheme for BP-CPT and the chemical structure of CPT-11 are shown in Fig. 1, A and B, respectively. Biotage FLASH 25+ column chromatography system was used to purify reaction products, and TLC was performed on silica gel plates (Merck TLC plate, silica gel 60 F254). Following purification, BP-CPT was homogeneous by TLC. ^{1}H Nuclear magnetic resonance (NMR) spectra were obtained using a Varian INOVA-500 (500 MHz) and chemical shifts are reported in parts/million (δ) relative to residual solvent peak or internal standard (tetramethylsilane) and coupling constants (J) are reported in Hz. Mass spectra were recorded on a Bruker Esquire liquid chromatography mass spectrometry using electrospray ionization. Spectroscopy afforded results consistent with the assigned structure.

Active Site Molecular Docking

For ligand-receptor docking, docking experiments were performed using the program Genetic Optimization for Ligand Docking (GOLD) to dock compounds into the active site of the rCE. GOLD uses a genetic algorithm to examine the ligand's conformational flexibility (20). Structural coordinates for rCE were provided by Bencharit *et al.* (21; PDB code 1K4Y). For molecular docking, the program was set to propose the 10 best solutions by GOLD score, and template molecules were docked into an active site volume of 10 Å.

Molecular Surface

The molecular surface property map in Fig. 2 of the rCE active site reflects lipophilic potential and was generated as the Connolly surface using the SYBYL-based MOLCAD program. The Connolly surface is essentially the portion of the van der Waals surface of a molecule that is accessible to solvent (22).

Molecular Modeling

All molecular modeling calculations and visualizations were performed using the molecular modeling program SYBYL 6.8 (23) on a Silicon Graphics Octane2 visual workstation running under the IRIX 6.5 operating system.

Data Sets

The initial training set consisted of 10 compounds comprising a series of camptothecin analogues having carbamate-linked side chains and differing principally in the substituents attached to the C-10 position of camptothecin. Input data were the negative logs of relative activity, with relative activity defined as the percent hydrolysis by rat serum esterase activity of each compound in the training set under the experimental conditions reported by Tsuji *et al.* (14). All analogues were constructed from the standard fragment library in SYBYL. Structures were energy minimized using the Tripos force field (24) with a distance-dependent dielectric and the Powell conjugate gradient algorithm with a convergence criterion of 0.001 kcal/mol Å. Partial atomic charges (Mulliken) of the molecules were calculated using the PM3 Hamilitonian model within MOPAC 6.0. (25).

Comparative Molecular Field Analysis and Comparative Molecular Similarity Index Analysis Studies: Alignment and Interaction Energy

Comparative molecular field analysis (CoMFA) is a mathematical expression of the correlation between the chemical structure of a series of compounds and the experimentally determined biological activities of these compounds (26). Comparative molecular similarity index analysis (CoMSIA) is an alternative molecular field analysis method to CoMFA. CoMSIA, like CoMFA, correlates the chemical structures with the biological activities of a set of compounds (27), but in addition to the

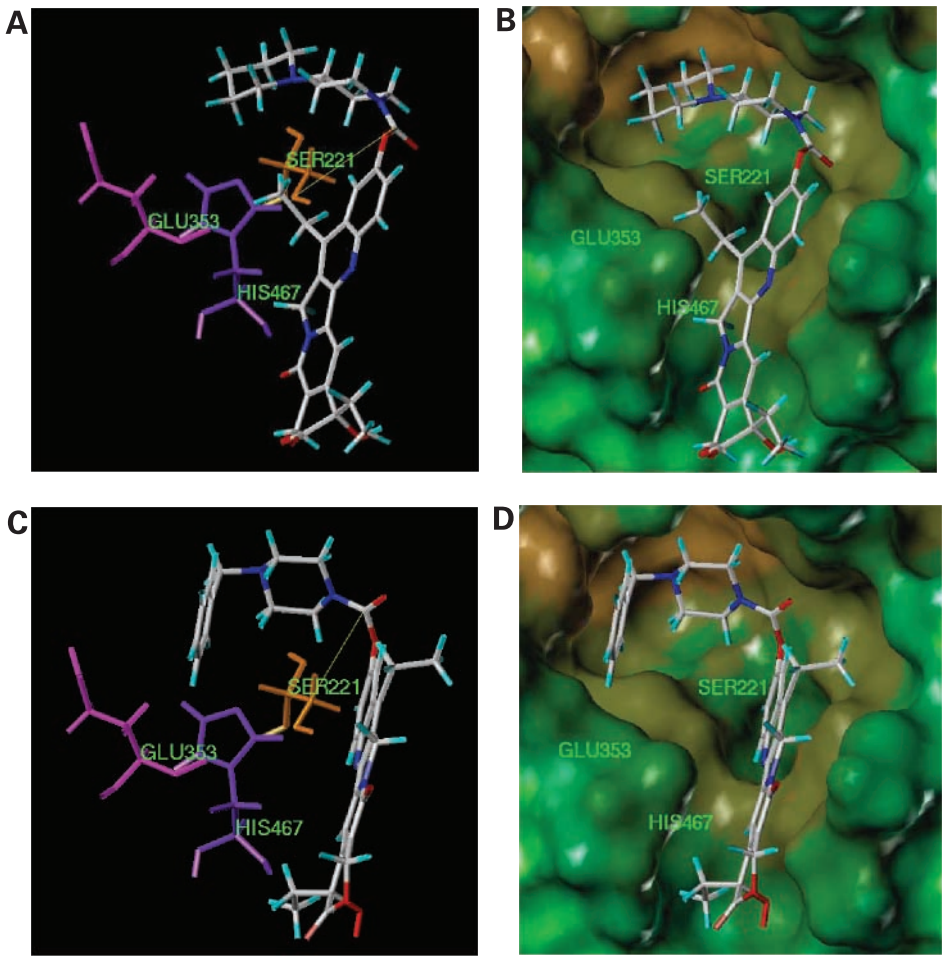

Figure 2. GOLD docking of CPT-11 and BP-CPT with the active site of rCE. **A** and **C,** stereoview of GOLD docking of the ligands (CPT-11 and BP-CPT) with rCE active site amino acid triad. The two prodrugs are colored by atom type (C, *white*; N, *blue*; and O, *red*). Active site amino acids are shown in *orange* (Ser-221), *magenta* (Glu-343), and *purple* (His-467). The distance between Ser-221 and the carbonyl carbon of each analog is shown as a *yellow line*. **B** and **D,** GOLD docking of ligands with the MOLCAD surface contour map of the rCE active site. *Brown surfaces* are relatively hydrophobic compared with *green surfaces*.

steric and electrostatic fields, CoMSIA also defines hydrophobic fields and hydrogen bond donor and acceptor fields and is used as an adjunct method to CoMFA.

CoMFA and CoMSIA studies require alignment of the three-dimensional structures of the molecules to be analyzed. SYBYL multifit alignment was used for the CoMFA and CoMSIA molecular alignment. For the alignment, the SN-38 moiety of compound **12**, one of the most active analogues reported by Tsuji *et al.*, was used as a template. Alignment of all 14 analogues using the five-membered SN-38 fragment as a template is shown in Fig. 3. Following the standard CoMFA procedure, each compound was inserted into a three-dimensional lattice with grid points set to 2 Å in x, y, and z directions. The steric and electrostatic potential energy fields were calculated at each grid point by summing the individual energy interactions between each atom and a probe represented by a sp^3 carbon with an effective radius of 1.53 Å and a charge of +1. The interaction energies measured for all of the molecules in a set were placed in rows of the QSAR molecular spreadsheet. The steric term represents van der Waals interactions and the coulombic term represents electrostatic interactions. The cutoff was set to 30 kcal/mol. To improve efficiency and reduce noise, column filtering was set to 2.0 kcal/mol.

Partial Least Squares Analysis

A partial least squares (PLS; 28) method was used to generate a linear regression equation to reflect differences in the steric and electrostatic CoMFA fields and to correlate these differences with differences in biological activities. The predictive ability of the CoMFA models was assessed using ''leave-one-out (LOO)'' cross-validation. For the LOO procedure, compounds were extracted one at a time from the data set, and the activity of the omitted compound was then predicted by a new model derived from the remaining compounds in the set. PLS (LOO) produced the optimum number of principal components and cross-validated correlation coefficient (q^2). A cross-validated correlation coefficient of 1 indicates no deviation between actual and predicted biological activities, while a coefficient of 0 indicates random correlation between chemical structure and its biological activity. The cross-validated q^2 reflects the degree to which model-predicted values match observed values. An acceptable lower limit for this value is 0.40, with a q^2 = 0.40–0.50 regarded as predictive and a $q^2 > 0.5$ as strongly predictive (29). The PLS was then repeated without cross-validation to produce a final model having a conventional correlation coefficient (r^2) to reflect the internal consistency of the model. Non-cross-validated analyses were used for

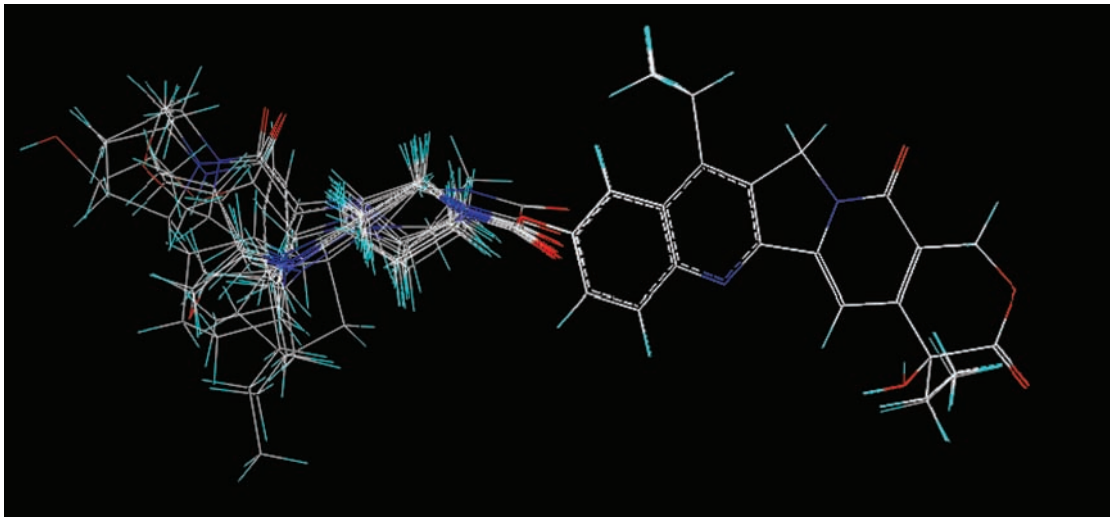

Figure 3. Molecular alignment of SN-38 prodrugs used in the CoMFA and CoMSIA modeling studies. All of the molecules were aligned using the SN-38 moiety of BP-CPT (compound **12**) as a template by multifit alignment using SYBYL program.

predictions reported in Table 1. The three-dimensional QSAR models are reported as CoMFA and CoMSIA contour maps that show the regions of steric and electrostatic fields of each model.

Cell Lines and Plasmids

U373MG glioma cells were purchased from the American Type Culture Collection (Bethesda, MD) and were grown in Dulbecco's MEM supplemented with 10% fetal bovine serum (Hyclone Laboratories, Logan, UT), 1-mM sodium pyruvate, 1-mM nonessential amino acids, and 2-mM L-glutamine in a humidified atmosphere of 10% CO_2 at 37°C. The mammalian expression vector pIRES (Clontech Laboratories, Inc., Palo Alto, CA) encoding rCE (30) or hiCE (31) was constructed as reported previously.

Transfection of Glioblastoma Cells

The method used to establish of U373pIRESneo, U373pIRESrCE, and U373pIREShiCE cell lines has been reported previously (11).

Growth Inhibition Assays

Growth inhibition experiments were also done as previously reported (8). Results are reported as the concentration of drug required to reduce cell number to 50% of untreated controls (IC_{50}; 32).

Determination of Kinetic Parameters for BP-CPT

K_m values and efficiency of production of SN-38 for BP-CPT with rCE, hiCE, and hCE1 were determined using baculovirus purified protein, as published (33). Briefly, 500 units of enzyme (1 unit is the amount of enzyme required to convert 1 μmol of *o*-nitrophenyl acetate to *o*-nitrophenol) were incubated with increasing concentrations of BP-CPT for 10 min at 37°C. The amount of SN-38 in each sample was determined using reverse-phase high-performance liquid chromatography (32). K_m values were calculated from hyperbolic plots using GraphPad Prism software.

Results

Synthesis of BP-CPT

Synthesis of the 4-benzylpiperazine derivative of CPT-11, BP-CPT, was accomplished using SN-38 as a starting material (Fig. 1A). To a stirring solution of SN-38 (11 mg, 0.027 mmol), pyridine (0.05 ml, 0.6 mmol) in dichloromethane (2 ml), triphosgene (14 mg, 0.047 mmol) was added under argon atmosphere. After 1 h stirring at room temperature, TLC was used to confirm that reaction was complete. 1-Benzylpiperazine (0.03 ml, 0.08 mmol) and pyridine (0.025 ml, 0.3 mmol) were then added to the mixture, and the reaction mixture was stirred for 6 h at room temperature (25°C). Dichloromethane was removed under reduced pressure and the crude product was purified by column chromatography using chloroform:methanol (9:1) to give a light brown oil (7 mg, 66%). TLC $R_f = 0.4$ (chloroform:-methanol, 97:3); ^{1}H NMR (500 MHz, $CDCl_3$) δ 0.98 (t, 3H, J = 1.4 Hz, CH_2CH_3), 1.40 (t, 3H, J = 1.4 Hz, CH_2CH_3), 1.6 (br s, 1H, OH), 2.4 (m, 2H, CH_2CH_3), 2.56 (m, 4H, N-CH_2 × 2), 3.15 (q, 2H, J = 1.4 Hz, pyr-CH_2CH_3), 3.60 (s, 2H, CH_2CH_3), 3.63 (br s, 2H, N-CH_2), 3.78 (br s, 2H, N-CH_2), 5.22 (dd, 2H, J = 2.3 and 4.6 Hz, CH_2), 5.40 (d, 1H, J = 4.6 Hz, CH), 5.67 (d, 1H, J = 4.6 Hz, CH), 7.24–7.35 (m, 5H, ph-H5), 7.6 (dd, 1H, J = 2.3 and 0.7 Hz, ph-H), 7.85 (d, 1H, J = 0.7 Hz, ph-H), 8.21 (d, 1H, J = 2.3 Hz, ph-H); MS (electrospray ionization) m/z 593 (M^- - 1, 100%), 549 (M^- - CO_2, 38%). The structure of CPT-11 is also shown for comparison (Fig. 1B).

Molecular Docking

Molecular docking studies were performed using GOLD to identify potential three-dimensional intermolecular interactions that determine or contribute to prodrug binding by the target enzyme rCE.

Hydrolysis of substrates by rCE is known to involve Ser-221, one of the members of the amino acid triad (Ser-221,

Table 1. CoMFA/CoMSIA training (CPT-11, 1–9) and test (10–13) set

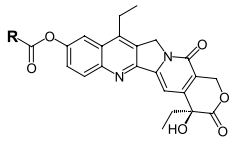

	Structure R	%RA[a]	Actual p(RA[a])	Predicted p(RA[a]) CoMFA	Predicted p(RA[a]) CoMSIA
CPT-11	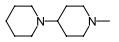	100	-2.000	-1.995	-1.995
1		50	-1.69897	-1.701	-1.701
2	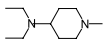	70	-1.8451	1.846	-1.849
3	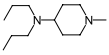	160	-2.20412	2.197	-2.186
4	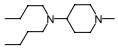	180	-2.25527	-2.260	-2.271
5	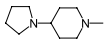	80	-1.90309	-1.904	-1.903
6	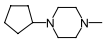	140	-2.14613	-2.151	-2.150
7	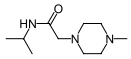	250	-2.39794	-2.398	-2.395
8	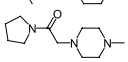	450	-2.65321	-2.654	-2.655
9	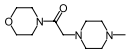	90	-1.95424	-1.953	-1.954
10	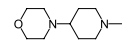	130	-2.11394	-1.854	-1.912
11	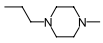	20	-1.30103	-1.968	-2.006
12	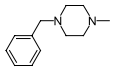	700	-2.8451	-1.907	-1.744
13	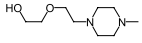	70	-1.8451	-2.229	-2.174

[a]Relative activity expressed in article by Tsuji *et al*. (14).

Glu-343, and His-467) conserved in CE active sites (21). The theoretical interaction between CPT-11 and BP-CPT and this triad of amino acids is shown in Fig. 2, A/B and C/D, respectively. In Fig. 2, A and C, the distance between Ser-221 and the carbonyl carbon of each prodrug is shown as a yellow line. In Fig. 2, B and D, the MOLCAD surface of the rCE catalytic site reflects the relative hydrophobic potential of the surface of this site. Regions in brown are relatively hydrophobic compared with regions in green. Interestingly, the SN-38 moiety common to both CPT-11 and BP-CPT docked into the active site in a similar orientation. However, the carbonyl carbon of BP-CPT was closer by 2.1 Å to the Ser-221 hydroxyl group than was the carbonyl carbon of CPT-11. It was unknown whether this closer proximity of the BP-CPT to Ser-221 would be more likely to facilitate hydrolysis of the prodrug or to stabilize the enzyme/prodrug complex, thereby decreasing the efficiency of hydrolysis of the prodrug.

Three-Dimensional QSAR Analysis

Three-dimensional QSAR studies were then performed using previously reported CPT-11 analogues and biological activity correlates to determine whether three-dimensional QSAR studies could be used in conjunction with docking studies to facilitate the design of CPT-11 prodrugs for specific esterases. We performed both CoMFA and CoMSIA analyses.

CoMFA. The model was based on the relative activity values reported by Tsuji *et al.* (14) of 10 compounds (CPT-11 plus nine analogues) for the training set and 4 compounds for the test set, as shown in Table 1. The SN-38 portions of all 14 molecules were superimposed (Fig. 3), and then all of the compounds were evaluated by CoMFA and CoMSIA analyses. The negative log of the actual and the CoMFA- and CoMSIA-predicted relative rates of hydrolysis of each compound are also shown in Table 1. Interestingly, both CoMFA and CoMSIA models predicted reasonable values for all of the compounds, except BP-CPT. BP-CPT showed ~1 log unit discrepancy for both models. These data suggested that, in contrast to published biological data, BP-CPT would be predicted to be hydrolyzed less efficiently than CPT-11 by rat serum esterase activity. This apparent discrepancy is considered further in ''Discussion.''

The statistical parameters for predicted CoMFA values are shown in Table 2. Based on steric plus electrostatic properties, PLS analysis gave a cross-validated q^2 correlation coefficient of 0.528 with an optimum number of six components and conventional non-cross-validated correlation coefficient of $r^2 = 1$. The contribution of steric parameters exceeded that of the electrostatic component, such that analysis using the steric parameter alone as the primary descriptor gave a higher cross-validated q^2 (0.583) than that observed when both steric and electrostatic properties were combined. The data suggest that the steric descriptor predominates in this structure-activity relationship model.

CoMSIA. CoMSIA analysis was performed using the same PLS protocol and procedure as was used for CoMFA. The same set of 14 compounds was used to evaluate the predictive power of CoMSIA models using steric, electrostatic, hydrophobic, and hydrogen donor and acceptor as descriptors. Predicted CoMSIA values were similar to predicted CoMFA values for all compounds.

Table 2. CoMFA statistical values

	Steric plus electrostatic	Steric	Electrostatic
q^{2a}	0.528	0.583	0.183
Component[b]	6	6	1
r^{2c}	1	1	1
SE[d]	0.006	0.004	0.011
F^e	2883	6643	1005

[a]Cross-validated correlation coefficient.
[b]Optimum number of components.
[c]Non-cross-validated (conventional) correlation coefficient.
[d]SE of estimate.
[e]F ratio.

Table 3. CoMSIA statistical values

	Steric	Electrostatic	Hydrophobic	Hydrogen D[a] + A[b]	Steric plus electrostatic
q^{2c}	0.656	0.126	0.678	−0.065	0.440
Component[d]	3	5	5	1	5
r^{2e}	0.997	1	0.998	0.978	0.999
SE[f]	0.028	0.005	0.023	0.072	0.015
F[g]	160	4213	233	23	557

[a]Donor.
[b]Acceptor.
[c]Cross-validated correlation coefficient.
[d]Optimum number of components.
[e]Non-cross-validated (conventional) correlation coefficient.
[f]SE of estimate, measure of the unexplained uncertainty.
[g]F ratio.

Statistical analysis of the predictive CoMSIA data is shown in Table 3. Also similar to CoMFA analysis, a primary descriptor of steric plus electrostatic parameters gave a lower q^2 value than did steric properties alone. PLS analysis of the CoMSIA values for compounds in the training set resulted in q^2 value of 0.440 and r^2 value of 0.999 for both parameters and a q^2 value of 0.656 and r^2 value of 0.997 for the steric descriptor alone. The hydrophobic descriptor also produced a good/excellent q^2 value of 0.678 and r^2 value of 0.998. Taken together, CoMFA and CoMSIA results suggest that steric properties may most accurately predict the biological activity of this class of prodrugs, with the hydrophobicity of the compound also a possible contributing factor.

CoMFA Contour Maps

The visual outcomes from CoMFA studies to correlate chemical structures with biological activities are depicted as three-dimensional contour maps. CoMFA steric and electrostatic maps with CPT-11 inserted for visual clarity are shown in Fig. 4, A–C. The field values were calculated at each grid point as the products of the QSAR coefficient and the SD of all values in the corresponding column of the data table (SD × coefficient). These values were plotted as a percentage contribution to the QSAR equation. The individual contributions from the steric and electrostatic fields were 80%/20% and 80%/20% for steric and electrostatic fields, respectively.

CoMFA steric contour maps show regions with potentially favorable (green) or unfavorable (yellow) effects of additional bulky groups on the biological activity of an analogue. The green contours in Fig. 4 around the second piperidino ring distal to the SN-38 moiety indicate that additional bulky groups in this position might enhance the biological activity of similar analogues. In contrast, yellow contours indicate that bulky groups in this region might result in steric hindrance and decreased biological activity. Blue contours in Fig. 4 indicate that the additional positively charged groups in this region may enhance biological activity. In contrast, there are also regions (red contours) where negatively charged groups may enhance biological activity. Interestingly, the model predicts that potential favorable changes to the prodrug molecules may be introduced only in regions adjacent to the second piperidino ring.

CoMSIA Contour Maps

The CoMSIA steric and electrostatic contour maps, similar to those shown for CoMFA, are represented in Fig. 5, A–C. The orange contours in the steric field represent sterically favored groups, and cyan indicates sterically disfavored. The magenta contours between the first and the second piperidino rings represent a region in which positively charged groups are favored, and the white contours indicate an area where negatively charged groups are favored. Similar to CoMFA contour maps in Fig. 4, CoMSIA maps indicated that efficient prodrug activation can be maintained only by restricting changes to these molecules to the groups distal to the first piperidino ring. Further, taken together, the above CoMFA and CoMSIA results (Figs. 3, 4, and 5; Tables 2 and 3) also suggested that the size and shape of groups in the region occupied by the second ring of CPT-11 are a primary determinant of efficiency of enzymatic activation of this class of prodrugs and, more specifically, that BP-CPT would be activated less efficiently than CPT-11 by rCE. To test these predictions, two types of biological studies were performed: growth inhibition assays and kinetic studies.

Growth Inhibition by CPT-11 or BP-CPT Mediated by rCE or hiCE Expression

rCE was selected as the target enzyme in this study because its structural coordinates have been determined and it is the most efficient enzyme known to cleave the dipiperidino side chain at the C-10 of CPT-11, thereby activating this prodrug.

U373MG human glioma cell lines were stably transfected with the control pIRES plasmid or this plasmid containing the cDNA that encodes rCE, and growth inhibition assays were performed. Each cell line was exposed to a range of concentrations of CPT-11 or BP-CPT for 4 h and growth inhibition curves and IC_{50} values were determined (Fig. 6; Table 4). The IC_{50} of the two drugs in

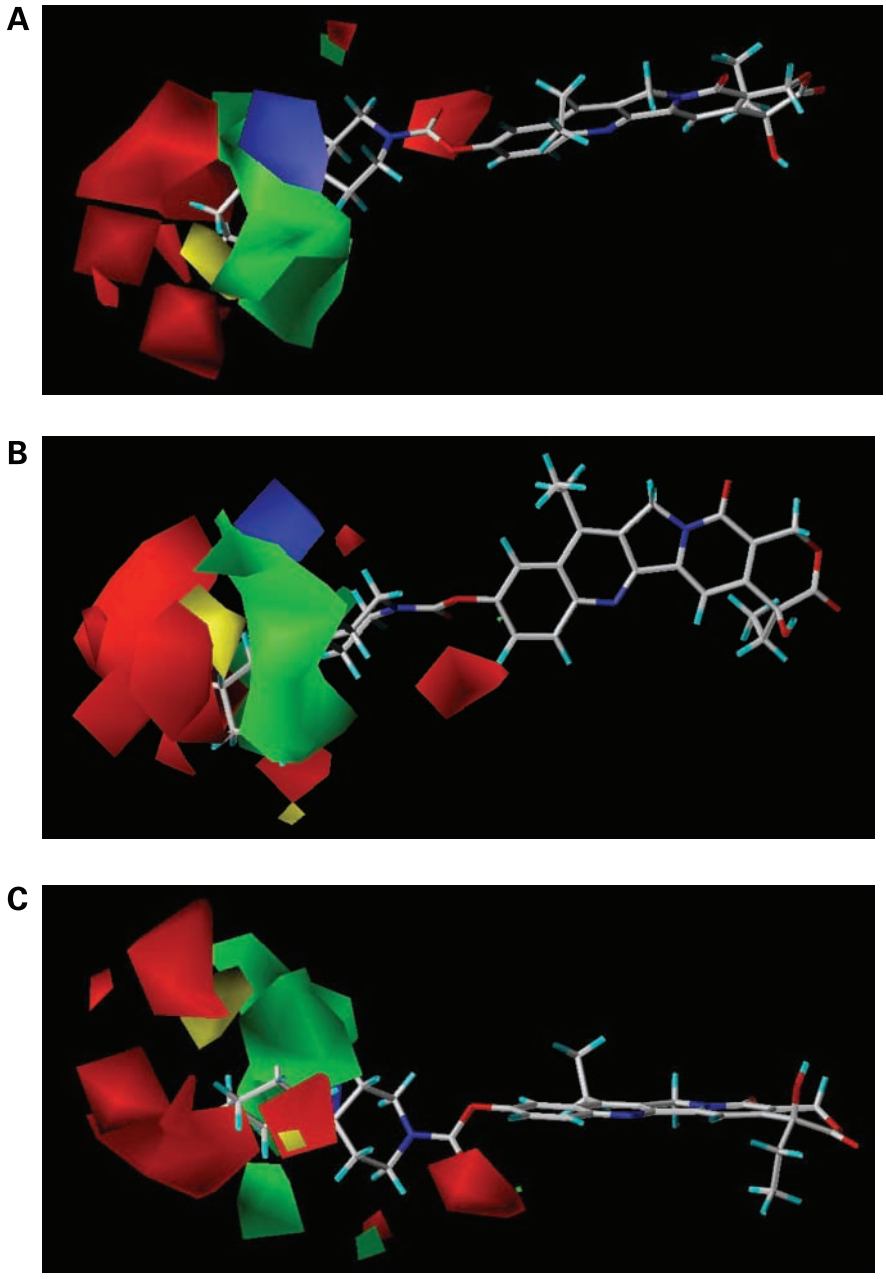

Figure 4. CoMFA contour maps for the (**A**) top, (**B**) side, and (**C**) bottom view of CPT-11. These steric and electrostatic CoMFA contour maps indicate the regions around the prodrug where a change in the field parameters affects the biological activity. If additional steric bulk is predicted to enhance activity, the contours are *green*. If steric bulk would likely decrease activity, contours appear *yellow*. *Blue* and *red* indicate regions where an increase in positive or negative charge, respectively, would enhance activity.

the vector-transfected U373pIRESneo cells differed only by a factor of 2.4. Because the hydrophobicity of the two compounds is similar (with ClogP values of 2.727 for CPT-11 and 3.786 for BP-CPT), these results suggested that the intracellular accumulation and activation of the two compounds in control cells with low CE levels were similar. In contrast, rCE expression in U373pIRESrCE cells decreased the IC_{50} values for CPT-11 and BP-CPT by ~276- and 23-fold, respectively, supporting the hypothesis that like CPT-11, BP-CPT is a prodrug that is activated by rCE. This result also indicates that rCE activated BP-CPT less efficiently than it activated CPT-11.

Further, because the ability of endogenous human enzymes to activate prodrugs is a factor in determining the suitability of prodrugs for VDEPT applications, it was also of interest to determine whether human CEs activate BP-CPT. Therefore, we transfected U373MG cells with the cDNA encoding hiCE and compared the relative ability of hiCE to activate the two prodrugs in growth inhibition assay. hiCE expression decreased the IC_{50} of CPT-11 by 11-fold but decreased the IC_{50} of BP-CPT by only ~2-fold, indicating that hiCE converted BP-CPT to SN-38 less efficiently than it converted CPT-11. Using the fold change in IC_{50} for CPT-11 in the U373pIRESneo cell line as a basis for comparison (23/276 for rCE compared with 2/11 for hiCE), the data also suggested that BP-CPT is a better substrate for rCE than for hiCE and support the hypothesis that it may be possible to identify substrates that interact selectively with specific CEs.

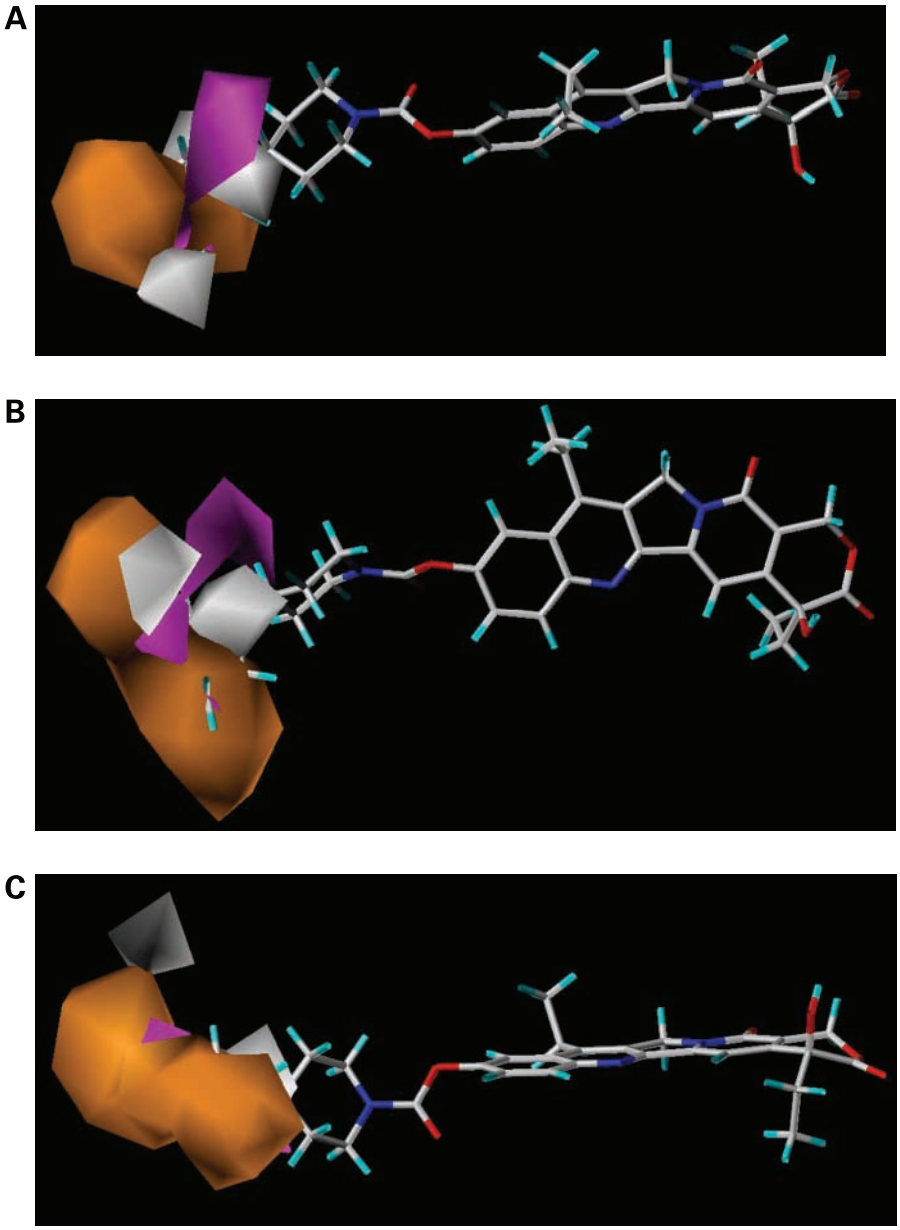

Figure 5. CoMSIA contour maps for the (**A**) top, (**B**) side, and (**C**) bottom view of CPT-11. *Orange* regions are those in which additional bulky groups would be expected to enhance activation of prodrugs, whereas presence of steric bulk in *cyan* regions would decrease activity. *Magenta* and *white* indicate regions in which an increase in positive or negative charge, respectively, would enhance activity.

Kinetic Parameters Support Modeling and Growth Inhibition Data

CoMFA/CoMSIA analyses based on the published biological data predicted that BP-CPT would likely be a relatively poor substrate for rCE compared with CPT-11 (Table 1). Growth inhibition data supported this prediction in that BP-CPT was 28-fold less potent than CPT-11 in inhibiting the growth of glioma cells transfected to express rCE. Because the active moiety of both CPT-11 and BP-CPT is SN-38, the growth inhibition experiments suggest that more CPT-11 than BP-CPT is converted to SN-38 by rCE. To confirm these results, the K_m of CPT-11 and BP-CPT for rCE and the efficiency of SN-38 production from each prodrug by rCE were determined (Table 5). The K_m values for CPT-11 and BP-CPT with rCE were 6.2 and 19.8 μM, respectively, and the yield of SN-38 produced (pmol/h/mg CE protein) were 18,963 and 813, respectively. Similar to results of modeling and growth inhibition experiments, these data suggest that BP-CPT is a poorer substrate for rCE than CPT-11. Additionally, while the structural coordinates of hiCE and hCE1 have not been determined, it would be essential for the intended VDEPT applications that potential prodrugs be metabolized less efficiently by hiCE and hCE1 than by rCE. Therefore, we also determined the K_m and catalytic efficiency of BP-CPT with hiCE and hCE1. Data in Table 5 show that the K_m for hCE1 is >500 μM, suggesting that BP-CPT would not be considered a substrate for hCE1. As expected, the production of SN-38 by hCE1 *in vitro*, under ideal conditions, was only 75 pmol/h/mg CE protein. In

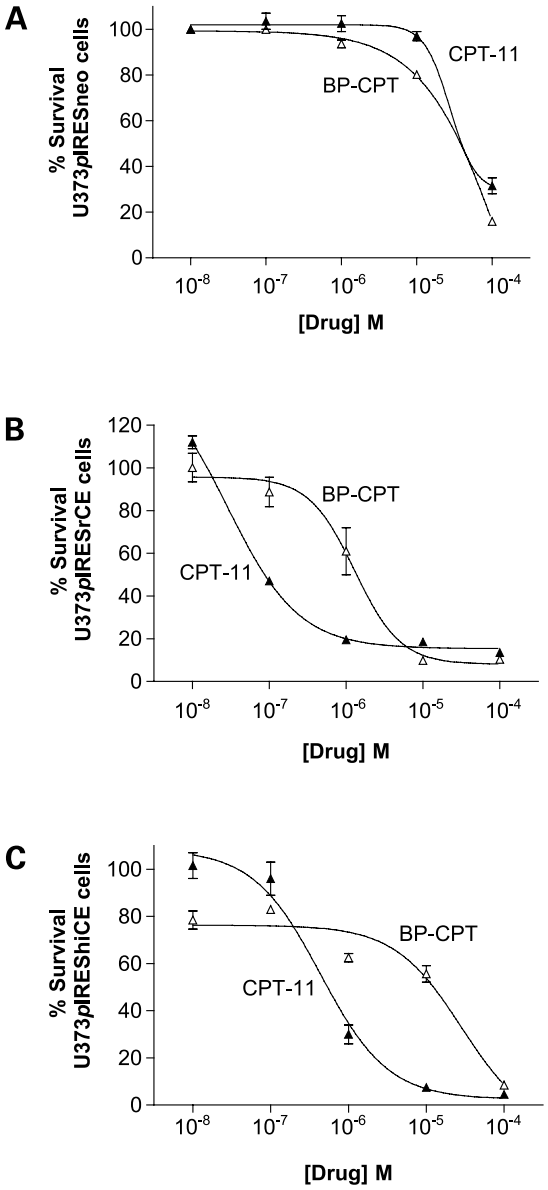

Figure 6. Growth inhibition curves for CPT-11 and BP-CPT for U373MG cells transfected with (**A**) empty vector, (**B**) rCE, and (**C**) hiCE cDNA. Drug exposure was for 4 h. The number of cells was quantitated five cell doubling times thereafter. *Points,* means of duplicate points in two to three separate experiments; *bars,* SEM. rCE activates CPT-11 more efficiently than any other known enzyme. hiCE is the most efficient human enzyme known to activate CPT-11. U373pIRESneo cells express ~10 units of endogenous CE activity. U373pIRESrCE cells express ~1000 units of rCE activity. U373pIREShiCE cells express ~200 units of hiCE activity. Therefore, IC_{50} values for each drug with U373pIRESrCE and U373pIREShiCE can be compared directly with U373pIRESneo cells to evaluate the effect of rCE or hiCE expression on prodrug potency, but IC_{50} values for U373pIRESrCE and U373pIREShiCE cannot be compared directly with each other.

contrast, BP-CPT had a higher affinity for hiCE than for rCE (with a K_m of 0.65 μM compared with 6.2 μM for rCE); however, rCE produced ~3-fold more SN-38 than did hiCE under the same conditions. These results are consistent with growth inhibition data (Fig. 6). The IC_{50} of BP-CPT in U373pIREShiCE and U373pIRESneo were the same, indicating minimal activation of BP-CPT by hiCE *in situ*. The most likely explanation for the above data is, as has been proposed by Bencharit *et al.* (21), that CE reaction products exit the catalytic gorge of the enzyme through a ''backdoor.'' Potentially, the relatively high affinity of either BP-CPT or one of the reaction products of BP-CPT does not permit rapid release of molecules from the catalytic site, thereby decreasing the overall reaction velocity. This concept is considered in more detail in ''Discussion.''

Discussion

CEs are relatively promiscuous enzymes that metabolize many esters and carbamates (34, 35); however, relatively large substrates such as CPT-11 are metabolized by only a few enzymes of this class. We proposed that it might be possible to design prodrugs that are analogues of CPT-11 but are activated by specific esterases for use in gene therapy approaches to cancer treatment such as VDEPT or ADEPT. To this end, it would be useful to identify a molecular modeling ''system'' that would predict the ability of a specific enzyme to metabolize a specific prodrug. While the prodrug in this study (BP-CPT) was predicted and confirmed to be a poorer substrate than CPT-11 for rCE, our results demonstrate that the CoMFA/CoMSIA modeling method accurately predicted the relative ability of rCE to convert two ''SN-38 prodrugs'' to active moiety. This method is currently being used to design prodrugs specifically for VDEPT using rCE.

CoMFA and CoMSIA analyses demonstrated that steric factors were the best single predictor of biological activity of BP-CPT. In addition, because the docking models showed a similar orientation of the SN-38 moiety for CPT-11 and BP-CPT in the active site of rCE (Fig. 2), it is also likely that it is either the proximity or the angle of the carbonyl group on the side chain of the prodrug to the hydroxyl group of Ser-221 that determines the rate of hydrolysis by a specific CE. Interestingly, the carbonyl carbon of BP-CPT, which was predicted and determined by biological evaluation to be a worse substrate for rCE than CPT-11, lies closer to the active Ser-221 than the carbonyl carbon of CPT-11. This close interaction of BP-CPT and Ser-221 of rCE could either enhance or slow the rate of enzymatic turnover. More specifically, the K_m of 19.8-μM BP-CPT for rCE suggested that this prodrug binds reasonably well to the active site of the enzyme. However, the affinity of the reaction products

Table 4. IC_{50} values obtained from growth inhibition assay

	U373pIRESneo	U373pIRESrCE	U373pIREShiCE
CPT-11 (IC_{50}, μM)	22.1 ± 9.6	0.08 ± 0.008	2.1 ± 0.02
BP-CPT (IC_{50}, μM)	52.3 ± 17.7	2.3 ± 0.4	24.8 ± 10.1

Data were expressed as means ± SEM of triplicate experiments.

Table 5. Kinetic properties of CPT-11 and BP-CPT by rCE and hiCE

	Enzyme	K_m (μM)[a]	SN-38 (pmol/h/mg CE protein)
CPT-11	rCE	6.2	18,963
BP-CPT	rCE	19.5	813
	hiCE	0.65	326
	hCE1	>500	75

[a] K_m values were calculated from hyperbolic plots using GraphPad Prism software.

might hinder the conformational changes in the enzyme that have been proposed to be required to facilitate exit of one or both reaction products through the ''backdoor'' of the enzyme (21).

In this current work, we used data reported previously by Tsuji *et al.* (14) to predict the efficiency of activation of CPT-11 analogues by rCE. Before confirmation by growth inhibition assays and kinetic analyses, several factors were identified that could have limited the information that could be derived from the analysis. Firstly, the side chains attached to the SN-38 in the molecules reported by Tsuji *et al.* had large torsion angles and were very flexible. Secondly, a limited number of compounds were studied and it was unknown whether interpretable data would be derived from the small training/test sets. Thirdly, the CPT-11 converting enzyme isolated from rat serum by Tsuji *et al.* was only partially purified, possibly confounding reported results for enzymatic activity. With these potential limitations in mind but relying on the conserved natures of CEs, we used the structural coordinates for rCE to determine whether these previously published results would provide informative data on which to base molecular modeling studies for rCE. Our data demonstrate that the predictions obtained from the modeling experiments were validated by both growth inhibition studies and kinetic analyses. This is the first report on three-dimensional QSAR studies using a series of CPT-11 analogues, the side chains of which were modified. Of note, in apparent contrast to data reported by Tsuji *et al.* for a partially purified rat serum esterase activity, we observed that the amount of SN-38 produced from BP-CPT by rat serum was only 7.5% of that produced from CPT-11 (data not shown). CoMFA and CoMSIA analyses are consistent with the latter data.

Overall, the described three-dimensional QSAR approach appears to be a useful predictive model for the design of novel SN-38 prodrug.

Acknowledgment

We thank Dr. Shantaram Kamath for sharing his expertise in the GOLD program and helpful discussions on molecular modeling.

References

1. Fillat, C., Carrio, M., Cascante, A., and Sangro, B. Suicide gene therapy mediated by the herpes simplex virus thymidine kinase gene/ganciclovir system: fifteen years of application. Curr. Gene Ther., *3:* 13 – 26, 2003.

2. Shibata, M. A., Morimoto, J., and Otsuki, Y. Suppression of murine mammary carcinoma growth and metastasis by HSVtk/GCV gene therapy using *in vivo* electroporation. Cancer Gene Ther., *9:* 16 – 27, 2002.

3. Black, M. E., Kokoris, M. S., and Sabo, P. Herpes simplex virus-1 thymidine kinase mutants created by semi-random sequence mutagenesis improve prodrug-mediated tumor cell killing. Cancer Res., *61:* 3022 – 3026, 2001.

4. Wilder, O., Blaese, R. M., and Candotti, F. Enzyme prodrug gene therapy: synergistic use of the herpes simplex virus-cellular thymidine kinase/ganciclovir system and thymidylate synthase inhibitors for the treatment of colon cancer. Cancer Res., *59:* 5233 – 5238, 1999.

5. Corban-Wilhelm, H., Hull, W. E., Becker, G., Bauder-Wust, U., Greulich, D., and Debus, J. Cytosine deaminase and thymidine kinase gene therapy in a dunning rat prostate tumor model: absence of bystander effects and characterization of 5-fluorocytosine metabolism with ^{19}F-NMR spectroscopy. Gene Ther., *9:* 1564 – 1575, 2002.

6. Koyama, F., Sawada, H., Fujii, H., Hirao, T., Ueno, M., Hamada, H., and Nakano, H. Enzyme/prodrug gene therapy for human colon cancer cells using adenovirus-mediated transfer of the *Escherichia coli* cytosine deaminase gene driven by a CAG promoter associated with 5-fluorocytosine administration. J. Exp. Clin. Cancer Res., *19:* 75 – 80, 2000.

7. Wybranietz, W. A., Gross, C. D., Phelan, A., O'Hare, P., Spiegel, M., Graepler, F., Bitzer, M., Stahler, P., Gregor, M., and Lauer, U. M. Enhanced suicide gene effect by adenoviral transduction of a VP22-cytosine deaminase (CD) fusion gene. Gene Ther., *8:* 1654 – 1664, 2001.

8. Danks, M. K., Morton, C. L., Pawlik, C. A., and Potter, P. M. Overexpression of a rabbit liver carboxylesterase sensitizes human tumor cells to CPT-11. Cancer Res., *58:* 20 – 22, 1998.

9. Potter, P. M., Pawlik, C. A., Morton, C. L., Naeve, C. W., and Danks, M. K. Isolation and partial characterization of a cDNA encoding a rabbit liver carboxylesterase that activates the prodrug irinotecan (CPT-11). Cancer Res., *58:* 2646 – 2651, 1998.

10. Danks, M. K., Morton, C. L., Krull, E. J., Cheshire, P. J., Richmond, L. B., Naeve, C. W., Pawlik, C. A., Houghton, P. J., and Potter, P. M. Comparison of activation of CPT-11 by rabbit and human carboxylesterases for use in enzyme/prodrug therapy. Clin. Cancer Res., *5:* 917 – 924, 1999.

11. Satoh, T., Hosokawa, M., Atsumi, R., Suzuki, W., Hakusui, H., and Nagai, E. Metabolic activation of CPT-11, 7-ethyl-10-[4-(1-piperidino)-1-piperidino] carbonyloxycamptothecin, a novel antitumor agent, by carboxylesterase. Biol. Pharm. Bull., *17:* 662 – 664, 1994.

12. Wagner, L. M., Guichard, S. M., Burger, R. A., Morton, C. L., Straign, C. M., Ashmun, R. A., Harris, L. C., Houghton, P. J., Potter, P. M., and Danks, M. K. Efficacy and toxicity of a virus-directed enzyme prodrug therapy purging method: preclinical assessment and application to bone marrow samples from neuroblastoma patients. Cancer Res., *62:* 5001 – 5007, 2002.

13. Kawato, Y., Aonuma, M., Hirota, Y., Kuga, H., and Sato, K. Intracellular roles of SN-38, a metabolite of the camptothecin derivative CPT-11, in the antitumor effect of CPT-11. Cancer Res., *51:* 4187 – 4191, 1991.

14. Tsuji, T., Kaneda, N., Kado, K., Yokokura, T., Yoshimoto, T., and Tsuru, D. CPT-11 converting enzyme from rat serum: purification and some properties. J. Pharmacobiodyn., *14:* 341 – 349, 1991.

15. Schwer, H., Langmann, T., Daig, R., Becker, A., Aslanidis, C., and Schmitz, G. Molecular cloning and characterization of a novel putative carboxylesterase, present in human intestine and liver. Biochem. Biophys. Res. Commun., *233:* 117 – 120, 1997.

16. Humerickhouse, R., Lohrbach, K., Li, L., Bosron, W. F., and Dolan, M. E., Characterization of CPT-11 hydrolysis by human liver carboxylesterase isoforms hCE-1 and hCE-2. Cancer Res., *60:* 1189 – 1192, 2000.

17. Rivory, L. P., Chatelut, E., Canal, P., Mathieu-Boue, A., and Robert, J. Kinetics of the *in vivo* interconversion of the carboxylate and lactone forms of irinotecan (CPT-11) and of its metabolite SN-38 in patients. Cancer Res., *54:* 6330 – 6333, 1994.

18. Wood, J. L., Fortunak, J. M., Mastrocola, A. R., Mellinger, M., and Burk, P. L. An efficient conversion of camptothecin to 10-hydroxycamptothecin. J. Org. Chem., *60* (17)*:* 1995.

19. Yoon, K. J., Morton, C. L., Potter, P. M., Danks, M. K., and Lee, R. E. Synthesis and evaluation of esters and carbamates to identify critical functional groups for esterase-specific metabolism. Bioorg. Med. Chem., *11:* 3237 – 3244, 2003.

20. Jones, G., Willett, P., Glen, R. C., Leach, A. R., and Taylor, R. Development and validation of a genetic algorithm for flexible docking. J. Mol. Biol., *267:* 727 – 748, 1997.

21. Bencharit, S., Morton, C. L., Howard-Williams, E. L., Danks, M. K., Potter, P. M., and Redinbo, M. R. Structural insights into CPT-11 activation by mammalian carboxylesterases. Nat. Struct. Biol., *9:* 337 – 342, 2002.

22. Connolly, M. L. Analytical molecular surface calculation. J. Appl. Crystallogr., *16:* 548 – 558, 1983.

23. SYBYL, Version 6.8. St. Louis, MO: Tripos Associates, 2001.

24. Clark, M., Cramer, R. D., III, and Van Opdenbosch, N. The tripos force field. J. Comput. Chem., *10:* 982 – 1012, 1989.

25. Stewart, J. J. MOPAC: a semiempirical molecular orbital program. J. Comput. Aided Mol. Des., *4:* 1 – 105, 1990.

26. Cramer, R. D., Patterson, D. E., and Bunce, J. D. Comparative molecular field analysis (CoMFA). I. Effect of shape on binding of steroids to carrier proteins. J. Am. Chem. Soc., *110:* 5959 – 5967, 1988.

27. Kliebe, G., Abraham, U., and Mietzner, T. Molecular similarity indices in a comparative analysis (CoMSIA) of drug molecules to correlate and predict their biological activity. J. Med. Chem., *37:* 4130 – 4146, 1994.

28. Bush, B. L. and Nachbar, R. B., Jr. Sample-distance partial least squares: PLS optimized for many variables, with application to CoMFA. J. Comput. Aided Mol. Des., *7:* 587 – 619, 1993.

29. Collantes, E. R., Xing, L., Miller, P. C., Welsh, W. J., and Profeta, S. Comparative molecular field analysis as a tool to evaluate mode of action of chemical hybridization agents. J. Agric. Food Chem., *47:* 5245 – 5251, 1999.

30. Potter P. M., Wolverton, J. S., Morton, C. L., Wierdl, M., and Danks, M. K. Cellular localization domains of a rabbit and human carboxylesterase: influence on irinotecan (CPT-11) metabolism by the rabbit enzyme. Cancer Res., *58:* 3627 – 3632, 1998.

31. Watkins, R. M., Morton, C. L., Weeks, J. K., Oliver, L., Wierdl, M., Danks, M. K., and Potter, P. M. Structural constraints affect the metabolism of 7-ethyl-10-[4-(1-piperidino)-1-piperidino]carbonyloxycamptothecin (CPT-11) by carboxylesterases. Mol. Pharmacol., *60:* 355 – 362, 2001.

32. Guichard, S. M., Morton, C. L., Krull, E. J., Stewart, C. F., Danks, M. K., and Potter, P. M. Conversion of the CPT-11 metabolite APC to SN-38 by rabbit liver carboxylesterase. Cancer Res., *4:* 3089 – 3094, 1998.

33. Morton, C. L. and Potter, P. M. Comparison of *Escherichia coli*, *Saccharomyces cerevisiae*, *Pichia pastoris*, *Spodoptera frugiperda*, and COS7 cells for recombinant gene expression. Application to a rabbit liver carboxylesterase. Mol. Biotechnol., *16:* 193 – 202, 2000.

34. Huang, T. L., Szekacs, A., Uematsu, T., Kuwano, E., Parkinson, A., and Hammock, B. D. Hydrolysis of carbonates, thiocarbonates, carbamates, and carboxylic esters of α-naphthol, β-naphthol, and *p*-nitrophenol by human, rat, and mouse liver carboxylesterases. Pharm. Res., *10:* 639 – 648, 1993.

35. Huang, T. L., Shiotsuki, T., Uematsu, T., Borhan, B., Li, Q. X., and Hammock, B. D. Structure-activity relationships for substrates and inhibitors of mammalian liver microsomal carboxylesterases. Pharm. Res., *13:* 1495 – 1500, 1996.